GEOPHYSICAL RESEARCH LETTERS, VOL. 40, 4951–4956, doi:10.1002/grl.50945, 2013

Geographically versus dynamically defined boundary layer cloud regimes and their use to evaluate general circulation model cloud parameterizations

Christine C.W. Nam[1,2] and Johannes Quaas[1,2]

Received 24 July 2013; revised 5 September 2013; accepted 6 September 2013; published 19 September 2013.

[1] Regimes of tropical low-level clouds are commonly identified according to large-scale subsidence and lower tropospheric stability (LTS). This definition alone is insufficient for the distinction between regimes and limits the comparison of low-level clouds from CloudSat radar observations and the ECHAM5 GCM run with the COSP radar simulator. Comparisons of CloudSat radar cloud altitude-reflectivity histograms for stratocumulus and shallow cumulus regimes, as defined above, show nearly identical reflectivity profiles, because the distinction between the two regimes is dependent upon atmospheric stability below 700 hPa and observations above 1.5 km. Regional subsets, near California and Hawaii, for example, have large differences in reflectivity profiles than the dynamically defined domain; indicating different reflectivity profiles exist under a given large-scale environment. Regional subsets are better for the evaluation of low-level clouds in CloudSat and ECHAM5 as there is less contamination between 2.5 km and 7.5 km from precipitating hydrometeors which obscured cloud reflectivities. **Citation:** Nam, C. C.W., and J. Quaas (2013), Geographically versus dynamically defined boundary layer cloud regimes and their use to evaluate general circulation model cloud parameterizations, *Geophys. Res. Lett.*, *40*, 4951–4956, doi:10.1002/grl.50945.

1. Introduction

[2] Intercomparisons of General Circulation Models (GCM) have shown that intermodel spread in climate sensitivity is dominated by cloud feedbacks [*Soden and Held*, 2006; *Bony and Dufresne*, 2005]. The uncertainty in cloud feedbacks in turn is believed to be primarily due to low-level clouds [*Vial et al.*, 2013; *Webb et al.*, 2006; *Medeiros et al.*, 2008].

[3] Low-level clouds are oftentimes identified according to the large-scale dynamics [*Klein and Hartmann*, 1993; *Bony et al.*, 2004; *Wood and Bretherton*, 2006; *Medeiros and Stevens*, 2011]. Other times, geographical regions are used as a proxy for studying the representations of a cloud regime [*Webb et al.*, 2001; *Chepfer et al.*, 2010]. This study aims to evaluate the representation of low-level clouds in the ECHAM5 GCM using CloudSat radar observations using dynamically and geographically defined cloud regimes. Using ERA-Interim reanalysis [*Dee et al.*, 2011] alongside CloudSat observations [*Stephens et al.*, 2002] and the ECHAM5 GCM [*Roeckner et al.*, 2003] paired with the Cloud Feedback Model Intercomparison Project Observational Simulator Package ([*Bodas-Salcedo et al.*, 2011], COSP) radar simulator, the radar joint cloud altitude-reflectivity histograms of stratocumulus and shallow cumulus cloud regimes were compared. This was done for both the dynamically defined stratocumulus and shallow cumulus regimes and regional subsets off the coasts of California, Hawaii, Peru, Namibia, Barbados, and Madagascar. This led to some surprising results, more specifically, we found that the identification of low-level cloud regimes by large-scale dynamics alone is insufficient for spaceborne radar observations and radar satellite simulators. How we came to such a conclusion is presented below, beginning with a description of clouds in the ECHAM5 model, the COSP radar satellite simulator, as well as the CloudSat data in section 2. Our experiment description is presented in section 3; followed by the results and conclusions in sections 4 and 5, respectively.

2. Model and Data

2.1. Clouds in ECHAM5

[4] Clouds in the ECHAM5 atmospheric GCM are represented by a convective cloud scheme and stratiform cloud scheme. Convective clouds are represented by the *Tiedtke* [1989] mass-flux concept and bulk cloud model. Convection is separated into shallow, mid-level, and penetrative convection. Shallow convection develops when surface evaporation in a column is greater than the large-scale convergence of moisture. Penetrative convection occurs when the converse is true. Mid-level convection occurs when convection initiates above the boundary layer and a temperature inversion inhibits large-scale convergence at low levels. This work mainly focuses on low clouds, thus, the shallow and mid-level convection are of main interest. The cloud fraction attributed to convective clouds is assumed negligible in the radiation scheme, however, such clouds contribute to the stratiform cloud fraction via the detrainment of cloud water from convective updrafts [*Lohmann and Roeckner*, 1996].

[5] Stratiform clouds are represented by three components: prognostic equations for water vapor, cloud liquid, and ice water; a microphysical scheme; followed by a cloud cover scheme. The mass mixing ratios of water vapor, cloud liquid water, and cloud ice are prognostically calculated using the bulk cloud microphysics scheme presented in *Lohmann and Roeckner* [1996]. They are transported using a flux form semi-Lagrangian transport scheme [*Lin and Rood*, 1996]. The mixing ratios are used to calculate

Additional supporting information may be found in the online version of this article.

[1]Max Planck Institute for Meteorology, Hamburg, Germany.
[2]Institute for Meteorology, Universität Leipzig, Leipzig, Germany.

Corresponding author: C. C.W. Nam, University of Leipzig, Vor dem Hospitaltore 1, 04103 Leipzig, Germany. (christine.nam@uni-leipzig.de)

0094-8276/13/10.1002/grl.50945

the total water mixing ratio. Integrating over the saturated part of the subgrid-scale total water mixing ratio probability density function (PDF), whose shape is related to subgrid-scale processes such as turbulence and convection, the cloud fraction of a the model grid box is determined using the statistical cloud scheme of *Tompkins* [2002]. The cloud fraction of each grid box is then used in conjunction with the maximum random overlap assumption to derive a projected 2-D total cloud cover.

2.2. CloudSat Radar Simulator

[6] In this study, ECHAM5 is run with the COSP version 1.2.1 CloudSat radar simulator (QuickBeam, [*Haynes et al.*, 2007; *Bodas-Salcedo et al.*, 2011]). The satellite simulator takes the grid-column profile of pressure, temperature, cloud water content, cloud fraction, and precipitation flux from ECHAM5 and divides it into 50 subcolumns. The average hydrometeor fraction, which includes cloud and precipitation [*Marchand et al.*, 2009], over all the subcolumns equals the modeled grid averaged as hydrometeor fraction of each subcolumn equals zero or one [*Klein and Jakob*, 1999; *Chepfer et al.*, 2008]. Within the cloudy subcolumns, the in-cloud liquid water and ice content is assumed equal [*Klein and Jakob*, 1999]. Above each subcolumn, the satellite simulator mimics CloudSat radar signal. After accounting for both the model's maximum-random cloud-overlap assumption and the instrument sensitivity [*Chepfer et al.*, 2010], a histogram of equivalent reflectivity and altitude, based on a common definition as the CloudSat retrievals, is produced.

2.3. CloudSat Observations

[7] CloudSat is a polar orbiting satellite hosting a 94 GHz, near-nadir cloud radar. With a pulse of $\sim$ 3.3 μs, it provides a global view of the vertical profile of clouds and precipitation in the atmosphere, including the evolution and distribution of cloud liquid and ice contents with altitude [*Stephens et al.*, 2002]. Using the hydrometeors' reflectivities from the CloudSat Geometric Profile (2B-GeoProf) data set, CloudSat Reflectivity Data, available from the Institut Pierre Simon Laplace (IPSL) CLIMSERV group, are placed on a 2° by 2° latitude-longitude grid, with a vertical resolution of 480 m, consistent with the COSP simulator outputs.

3. Experiment Description

[8] In this paper, the stratocumulus and shallow cumulus cloud regimes in ECHAM5 are compared with CloudSat observations for the year 2007. The model is run in a T63L31 resolution (approx. 1.8° × 1.8° with 31 vertical levels), with prescribed monthly-mean sea surface temperature distribution and sea-ice cover distribution from the Atmospheric Model Intercomparison Project (AMIP2) as observed for the year 2007. After a 3 month spin-up period, a simulation with output data at a temporal resolution of 3 h for the full year 2007 was completed. The data were used to compute monthly means, for which the June-July-August (JJA) 2007 time period is presented here. This time period has been shown to be sufficient to evaluate model performance and identify model deficiencies [*Nam and Quaas*, 2012]. For an extended analysis of the entire 2007 period, as well as the regional comparisons of Peru, Namibia, Barbados, and Madagascar, please refer to the supporting information. Both these analyses demonstrate the spatial and temporal robustness of our analysis and corroborate our conclusions.

[9] The stratocumulus and shallow cumulus cloud regimes are classified according to the large-scale vertical velocity (ω), at 500 hPa and 700 hPa, and the lower tropospheric stability (LTS $\equiv \theta_{700\text{hPa}} - \theta_{\text{sfc}}$) [*Klein and Hartmann*, 1993; *Bony et al.*, 2004; *Medeiros and Stevens*, 2011]. The vertical velocities are first used to identify regions of large-scale subsiding motion, which are indicative of low-cloud regimes. These regions are then separated into stratocumulus and shallow cumulus cloud regimes using the LTS. Regions of strong subsidence are defined as areas where $\omega_{500\text{hPa}} \geq 10$ hPa d^{-1} and $\omega_{700\text{ hPa}} \geq 10$ hPa d^{-1} and LTS ≥ 18.55 K indicates stratocumulus while LTS < 18.55 K defines shallow cumulus [*Medeiros and Stevens*, 2011]. Within these two regimes we look at the regional subsets of the California Stratocumulus (15°–35°N; 110°W–140°W) and the Hawaiian Trade Cumulus (15°–35°N; 160°E–140°W following *Webb et al.* [2001].

[10] The observations combine CloudSat retrievals and European Centre for Medium-Range Weather Forecasts reanalysis data (ERA-Interim) from the JJA 2007 period. The monthly means of vertical velocity and potential temperature (θ) from ERA-interim were used to determine the large-scale dynamics of the atmosphere. For the analysis of the ECHAM model, both cloud and dynamics diagnostics are from the simulation itself.

4. Results

[11] The dynamical masks of ERA-Interim and ECHAM5, presented in Figure 1, show the areas where the conditions for stratocumulus and shallow cumulus regimes were satisfied within JJA 2007. The radar reflectivities from within the regions identified each month were used to create the joint cloud altitude-reflectivity histograms, commonly known as contoured frequency by altitude diagrams (CFAD) (Figure 2). The radar reflectivity histograms present the frequency of occurrence of clouds and precipitation in intervals of 480 m from 0 to 19.2 km for radar reflectivities from –30 dBZe to 20 dBZe. Radar reflectivities < –27.5 dBZe, have greater likelihood of false detection, therefore, hydrometeors are identified as particles with radar reflectivities > –27.5 dBZe following *Bodas-Salcedo et al.* [2008] and *Marchand et al.* [2009]. In addition, radar reflectivities below 1 km should be discarded due to ground clutter [*Tanelli et al.*, 2008; *Marchand et al.*, 2008]. The frequency of occurrence is normalized such that each altitude sums to one.

[12] Roughly speaking, the radar reflectivity histograms can be divided into four regions according to radar reflectivity and altitude of the hydrometeor. According to *Marchand et al.* [2009], hydrometeors above 5 km are predominantly composed of ice, and below 5 km, they are predominantly liquid. In *Nam and Quaas* [2012] radar reflectivities < –10 dBZe in ECHAM5 generally indicated nonprecipitating hydrometeors, whereas hydrometeors with ≥ –10 dBZe were generally precipitating. Note that radar reflectivities are dominated by larger particles, and in the presence of both precipitating and nonprecipitating hydrometeors, the radar reflectivity returned will be in the precipitating region of the histogram although nonprecipitating hydrometeors exist.

[13] The dynamical masks of both stratocumulus and shallow cumulus for ERA Interim and ECHAM5 are rather

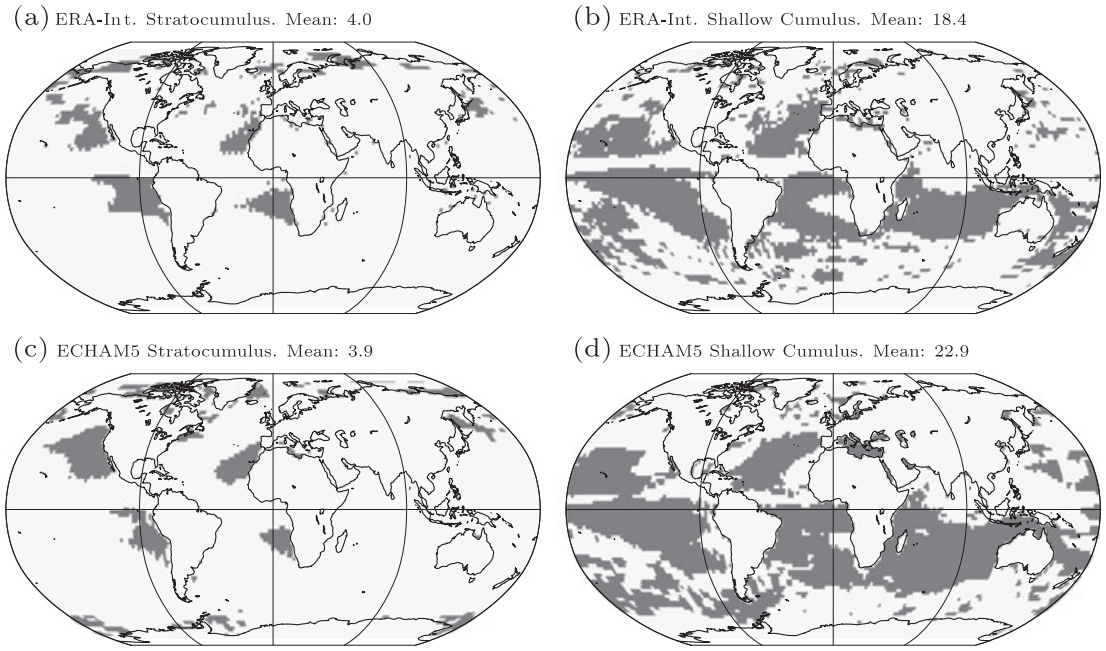

Figure 1. Dynamical masks show the areas where the conditions for stratocumulus and shallow cumulus regimes were satisfied within JJA 2007. (top row) ERA interim (a) stratocumulus; (b) shallow cumulus. (bottom row) ECHAM5 (c) stratocumulus; (d) shallow cumulus. Values indicate the averaged monthly mean area covered by each regime between 81°S–81°N.

similar in their geographical distributions and their averaged monthly means. Despite the similar dynamical masks, the resulting reflectivity histograms are very different (Figure 2b versus Figure 2c and Figure 2f versus Figure 2g). Not only are the dynamical radar histograms for CloudSat and ECHAM5 different from one another, they are vastly different to their regional counterparts (Figures 2a, 2d, 2e, 2h), which are oftentimes used to evaluate low-level cloud regimes in models *Webb et al.* [2001].

[14] Focusing on the reflectivity histograms of the stratocumulus and shallow cumulus regimes, in both observations and models, one can frequently see reflectivities associated with high-level and mid-level clouds as well as precipitating hydrometeors (Figures 2b, 2c, 2f, 2g). Despite

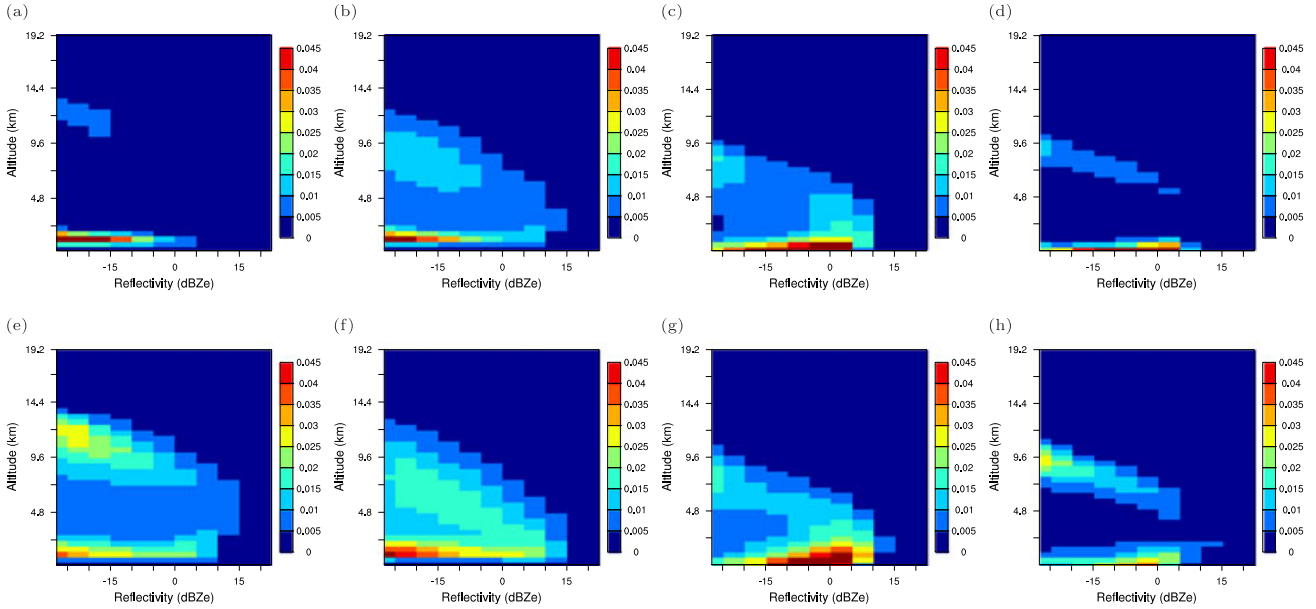

Figure 2. Radar cloud altitude-reflectivity histogram from dynamical regimes for JJA 2007. (top row) Stratocumulus: (a) Californian subset of CloudSat dynamical stratocumulus, (b) CloudSat dynamical stratocumulus, (c) ECHAM5 dynamical stratocumulus, (d) Californian subset of ECHAM5 dynamical stratocumulus. (bottom) Shallow Cumulus: (e) Hawaiian subset of CloudSat dynamical shallow cumulus, (f) CloudSat dynamical shallow cumulus, (g) ECHAM5 dynamical shallow cumulus, (h) Hawaiian subset of ECHAM5 dynamical shallow cumulus.

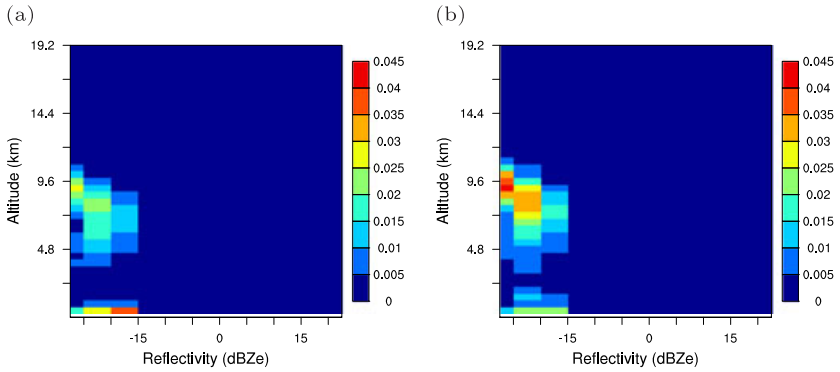

Figure 3. Radar cloud altitude-reflectivity histogram over the California and Hawaii regions when precipitation is withheld from simulator for July 2007.

having used subsiding motion to identify these two regimes, hydrometeors frequently occur in the upper troposphere. In both CloudSat retrievals and the ECHAM5 model, the stratocumulus and shallow cumulus reflectivity histograms look remarkably similar, with minor differences in the frequency of high-level cirrus clouds as well as mid-level clouds. The shallow cumulus regime shows a greater frequency of cirrus clouds and more mid-level hydrometeors compared to the stratocumulus regime. The overall similarity between reflectivity histograms of the two regimes can be traced back to the definition of the regimes themselves. It is only the LTS which distinguishes one low-cloud regime from the other. Unfortunately, the reflectivities below 700 hPa and above 1.5 km within the observations and models are remarkably similar, and in ECHAM5 the reflectivities are dominated by precipitating hydrometeors. It can be concluded that sampling solely according to these dynamical conditions is insufficient for distinguishing between stratocumulus and shallow cumulus clouds with satellite radar retrievals. The dynamically defined regimes are frequently influenced by precipitating hydrometeors, which obscures low-level cloud reflectivities.

[15] A comparison of reflectivity histograms of ECHAM5 (Figures 2c, 2g) to CloudSat (Figures 2b, 2f) show that within ECHAM5 the highest altitude of hydrometeors detected by the radar simulator is much lower than that found in CloudSat observations. This is because ECHAM5 underestimates the effective radius of ice particles, rendering high-level clouds undetected by the radar, while simultaneously overestimating the lidar scattering ratios when being evaluated with a lidar simulator [*Nam and Quaas*, 2012]. In the boundary layer, the greatest frequency of hydrometeors fall within the precipitating quadrant of the histogram. The mid-levels of ECHAM5 show a lower frequency of hydrometeors compared to CloudSat.

[16] The geographical subset off the Californian coast yields vastly different reflectivity histograms compared to the dynamically defined stratocumulus regime for both CloudSat and ECHAM5 (Figures 2a–2d). This holds true for the Peruvian and Namibian stratocumulus regions presented in the supporting information. The geographical subset off the Hawaiian coast also yields different reflectivity histograms compared to the dynamically defined shallow cumulus regime (Figures 2e–2h), although to a lesser extent. The differences between the regional subsets and the dynamical regimes mainly arise from precipitating hydrometeors as well as mid-level clouds. The Californian and Hawaiian subsets of CloudSat and ECHAM5 show a distinction between high-level cirrus and boundary layer clouds, which is not evident in the dynamically defined histograms.

[17] It can be concluded from the series of plots that not all stratocumulus and shallow cumulus regions, when defined dynamically according to *Medeiros and Stevens* [2011], have the same reflectivities signature despite having the same large-scale environmental properties. The observed regional subsets show very similar radar profiles as presented in *Marchand et al.* [2009], with a few high-level cirrus clouds overlying a relatively clear mid-level and an abundance of boundary layer hydrometeors. The greatest frequency of boundary layer hydrometeors occur in the non-precipitating quadrant of the histogram with clouds in the shallow cumulus regime more frequently reaching higher in the atmosphere compared to the stratocumulus regime.

[18] The reflectivity histograms of ECHAM5's Californian and Hawaiian subsets clearly show high-level hydrometeor reflectivities spanning into the precipitating quadrant of the histogram at a greater frequency than observed. Mid-level and low-level hydrometeors over the Californian and Hawaiian regions are frequently in the precipitating part of the histogram. In the lowest layers, the precipitating hydrometeors can obscure the few existing low-level clouds; motivating the sensitivity experiment in which precipitation

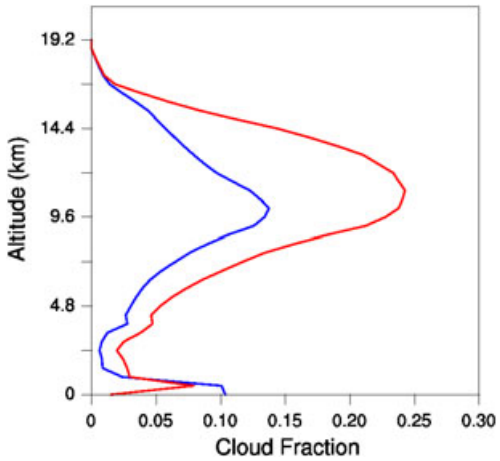

Figure 4. ECHAM5 cloud fraction profile over the Californian (blue) and Hawaiian (red) regions for JJA 2007.

is withheld from the radar simulator. The sensitivity experiment is designed to isolate the reflectivities of low-level clouds in ECHAM5 in the Californian and Hawaiian regions described above. We found that although low-level clouds in ECHAM5 are detected more frequently than in the control experiment, the frequency of occurrence remains significantly underestimated compared to CloudSat observations (Figure 3). In addition, the low-level clouds in ECHAM5 do not extend as high into the atmosphere as those in CloudSat. A look at the cloud fractions purely modeled by ECHAM5 in these two regions in Figure 4 shows that there are relatively few boundary layer clouds in these regions; motivating the need for a different boundary layer scheme in ECHAM5.

5. Conclusion

[19] This study found that the identification of tropical low-level cloud regimes according to the large-scale subsidence and lower tropospheric stability (LTS) is insufficient and limits the comparison of low-level clouds between CloudSat radar retrievals and the ECHAM5 GCM run with the COSP radar simulator. The radar reflectivity histograms of stratocumulus and shallow cumulus cloud regimes were found to be very similar as the distinction between the two regimes is solely dependent upon reflectivities below 700 hPa and above 1.5 km. This holds true for both CloudSat retrievals and the ECHAM5 GCM with the COSP radar simulator.

[20] The ECHAM5 radar reflectivity histograms showed a frequent presence of precipitating hydrometeors, as well as high-level clouds, throughout the atmosphere despite having used large-scale subsidence as a criteria for identifying the low-cloud regimes. Oftentimes, these higher-lying clouds and precipitating hydrometeors produced reflectivities that obscured those from the low-clouds and thus rendered the identification of boundary layer clouds according to the large-scale subsidence and lower tropospheric stability insufficient for comparison with satellite radar retrievals.

[21] Regional subsets near Hawaii and California, as well as those presented in the supporting information, were found to be better for the identification of low-level clouds using CloudSat retrievals as there was less contamination between 2.5 km and 7.5 km from precipitating hydrometeors; and similarly so for ECHAM5. Interestingly, the regional subsets have quite different reflectivity histograms compared to the dynamically defined domains. This implies that within a given large-scale environment, very different reflectivity profiles can exist. This is because the dynamical definitions capture more than the stratocumulus or shallow cumulus clouds themselves but other cloud types as well.

[22] The results drive home the need for improving the boundary layer scheme as well as the coupling of precipitation and clouds in the ECHAM5 parameterizations. There is also a need to develop creative methodologies for identifying low-level clouds from radar observations and synthesis of multisensor instrument observations for model evaluation. One such promising approach, shown by *Evans et al.* [2012], identifies unique hydrometeor occurrence profiles, from a ground-based millimeter vertically pointing radar, based on composites by atmospheric state. Application of such a technique to CloudSat retrievals and model data would be very interesting.

[23] **Acknowledgments.** Support for this work came from the International Max Planck Research School on Earth System Modelling, the German Research Foundation in an “Emmy Noether” grant and the European Union, Seventh Framework Programme (FP7/2007-2013) under grant agreement 244067 as well as the Federal Ministry of Education and Research in Germany (BMBF) through the research program High Definition Clouds and Precipitation for Climate Prediction - HD(CP)2 (FKZ: 01LK1210D). We would like to thank Alejandro Bodas-Salcedo from the MetOffice for sharing his knowledge regarding the CloudSat simulator as well as the two reviewers for providing constructive comments. We would also like to thank Bjorn Stevens, Sebastian Rast, Irene Stemmler, and Katrin Lonitz for fruitful discussions and technical help. Computing time has been provided by the German Climate Computing Centre (DKRZ). The satellite data used in this study came from the CloudSat satellite operated by NASA which has provided valuable observational data.

[24] The Editor thanks two anonymous reviewers for their assistance in evaluating this paper.

References

Bodas-Salcedo, A., M. J. Webb, M. E. Brooks, M. A. Ringer, K. D. Williams, S. F. Milton, and D. R. Wilson (2008), Evaluating cloud systems in the MetOffice global forecast model using simulated Cloudsat radar reflectivities, *J. Geophys. Res.*, *113*, D00A13, doi:10.1029/2007JD009620.

Bodas-Salcedo, A., et al. (2011), COSP: Satellite simulation software for model assessment, *Bull. Am. Meteorol. Soc.*, *92*, 1023–1043, doi:10.1175/2011BAMS2856.1.

Bony, S., and J. L. Dufresne (2005), Marine boundary layer clouds at the heart of tropical cloud feedback uncertainties in climate models, *Geophys. Res. Lett.*, *32*, L20806, doi:10.1029/2005GL023851.

Bony, S., J.-L. Dufresne, H. Le Treut, J.-J. Morcrette, and C. Senior (2004), On dynamic and thermodynamic components of cloud changes, *Clim. Dyn.*, *22*, 71–86, doi:10.1007/s00382-003-0369-6.

Chepfer, H., S. Bony, D. Winker, G. Cesana, J. Dufresne, P. Minnis, C. Stubenrauch, and S. Zeng (2010), The GCM Oriented CALIPSO Cloud Product (CALIPSO-GOCCP), *J. Geophys. Res.*, *115*, D00H16, doi:10.1029/2009JD012251.

Chepfer, H., S. Bony, D. Winker, M. Chiriaco, J. Dufresne, and G. Sèze (2008), Use of CALIPSO lidar observations to evaluate the cloudiness simulated by a climate model, *Geophys. Res. Lett.*, *35*, L15704, doi:10.1029/2008GL034207.

Dee, D. P., et al. (2011), The ERA-interim reanalysis: Configuration and performance of the data assimilation system, *Q. J. R. Meteorolog. Soc.*, *137*, 553–597, doi:10.1002/qj.828.

Evans, S., R. Marchand, T. Ackerman, and N. Beagley (2012), Identification and analysis of atmospheric states and associated cloud properties for Darwin, Australia, *J. Geophys. Res.*, *117*, D06204, doi:10.1029/2011JD017010.

Haynes, J., R. Marchand, Z. Luo, A. Bodas-Salcedo, and G. Stephens (2007), A multipurpose radar simulation package: Quickbeam, *Bull. Am. Meteorol. Soc.*, *88*, 1723–1727.

Klein, S., and D. Hartmann (1993), The seasonal cycle of low stratiform clouds, *J. Clim.*, *6*, 1587–1606.

Klein, S., and C. Jakob (1999), Validation and sensitivities of frontal clouds simulated by the ECWMF model, *Mon. Wea. Rev.*, *127*, 2514–2531.

Lin, S. J., and R. B. Rood (1996), Multidimensional flux form semi-Lagrangian transport, *Mon. Wea. Rev.*, *124*, 2046–2068.

Lohmann, U., and E. Roeckner (1996), Design and performance of a new cloud microphysics scheme developed for the ECHAM4 general circulation model, *Clim. Dyn.*, *12*, 557–572.

Marchand, R., J. Haynes, G. Mace, T. Ackerman, and G. Stephens (2009), A comparison of simulated cloud radar output from the multiscale modeling framework global climate model with Cloudsat cloud radar observations, *J. Geophys. Res.*, *114*, D00A20, doi:10.1029/2008JD009790.

Marchand, R., G. Mace, T. Ackerman, and G. Stephens (2008), Hydrometeor detection using Cloudsat—An Earth-orbiting 94-GHZ cloud radar, *J. Atmos. Oceanic Technol.*, *25*, 519–533.

Medeiros, B., B. Stevens, I. M. Held, M. Zhao, D. L. Williamson, J. G. Olson, and C. S. Bretherton (2008), Aquaplanets, climate sensitivity, and low clouds, *J. Clim.*, *21*, 4974–4991, doi:10.1175/2008JCLI1995.1.

Medeiros, B., and B. Stevens (2011), Revealing differences in GCM representations of low clouds, *Clim. Dyn.*, *36*, 385–399, doi:10.1007/s00382-009-0694-5.

Nam, C., and J. Quaas (2012), Evaluation of clouds and precipitation in the ECHAM5 general circulation model using CALIPSO and CloudSat satellite data, *J. Clim.*, *25*, 4975–4992, doi:10.1175/JCLI-D-11-00347.1.

Roeckner, E., et al., (2003), The atmospheric general circulation model ECHAM5: Part 1. REPORT 349. *Tech. rep., Max Planck Institute for Meteorology*, Hamburg, Germany. ISSN 0937–1060.

Soden, B. J., and I. M. Held (2006), An assessment of climate feedbacks in coupled ocean-atmosphere models, *J. Clim.*, *19*, 3354–3360, doi:10.1175/JCLI3799.1.

Stephens, G. L., et al. (2002), The Cloudsat mission and the A-train: A new dimension to space-based observations of clouds and precipitation, *Bull. Am. Meteorol. Soc.*, *83*, 1771–1790.

Tanelli, S., S. Durden, E. Im, K. Pak, D. Reinke, P. Partain, R. Marchand, and J. Haynes (2008), Cloudsats cloud profiling radar after 2 years in orbit: Performance, external calibration, and processing, *IEEE Trans. Geosci. Remote Sens.*, *46*(11), 3560–3573.

Tiedtke, M. (1989), A comprehensive mass flux scheme for cumulus parameterization in large-scale models, *Mon. Wea. Rev.*, *117*, 1779–1800.

Tompkins, A. M. (2002), A prognostic parameterization for the subgrid-scale variability of water vapor and clouds in large-scale models and its use to diagnose cloud cover, *J. Atmos. Sci.*, *59*, 1917–1942.

Webb, M., C. Senior, S. Bony, and J.-J. Morcrette (2001), Combining ERBE and ISCCP data to assess clouds in the Hadley centre, ECWMF and LMD atmospheric climate models, *Clim. Dyn.*, *17*(12), 905–922.

Webb, M. J., et al. (2006), On the contribution of local feedback mechanisms to the range of climate sensitivity in two GCM ensembles, *Clim. Dyn.*, *27*, 17–38.

Wood, R., and C. Bretherton (2006), On the relationship between stratiform low cloud cover and lower-tropospheric stability, *J. Clim.*, *19*, 6425–6432.

Vial, J., S. Bony, and J.-L. Dufresne (2013), On the interpretation of inter-model spread in CMIP5 climate sensitivity estimates, *Climate Dynamics*, doi:10.1007/s00382-013-1725-9.